Signature splitting and quasiparticle alignment in the yrast band of ^{165}Ta

D. G. Roux,[1,2] M. S. Fetea,[1] E. Gueorguieva,[1] B. R. S. Babu,[1,*] R. T. Newman,[1] J. J. Lawrie,[1] R. Fearick,[2] D. G. Aschman,[2] R. Beetge,[2] M. Benatar,[2] G. K. Mabala,[1] S. M. Mullins,[1] S. H. T. Murray,[2] S. Naguleswaran,[1,†] C. Rigollet,[1,‡] J. F. Sharpey-Schafer,[1] F. D. Smit,[1] and W. J. Whittaker[2]

[1]*National Accelerator Centre, P.O. Box 72, 7131 Faure, South Africa*

[2]*Department of Physics, University of Cape Town, Private Bag, 7701 Rondebosch, South Africa*

(Received 1 September 2000; published 8 January 2001)

Excited states in ^{165}Ta were populated in the ^{142}Nd(^{27}Al,4n)^{165}Ta and ^{141}Pr(^{28}Si,4n)^{165}Ta reactions and investigated using the AFRODITE array. The yrast rotational decay sequence up to spin $53/2^-$ is identified and assigned to the $[514]9/2^-$ configuration. The nuclear shape is investigated using total Routhian surface calculations. The experimental results are discussed in relation to existing data in the neighboring Ta isotopes and results from cranked shell model calculations. Unexpectedly large signature splitting, for a high-Ω configuration, is observed in the yrast band. Further discrepancies are observed between theoretical and experimental values for the band crossing frequency and signature splitting of the $B(M1)/B(E2)$ ratios. The possibility that these discrepancies are a consequence of a large deviation from an axially symmetric nuclear shape is investigated.

DOI: 10.1103/PhysRevC.63.024303 PACS number(s): 21.10.Re, 23.20.Lv, 25.70.Hi, 27.70.+q

I. INTRODUCTION

Nuclei in the $A\sim160$ mass region have shown a number of phenomena that challenge our understanding of nuclear structure. These rare-earth nuclei are known to have medium prolate deformation $\beta_2\sim0.1$–0.3 [1] and to exhibit rotational bands built on different multiquasiparticle orbitals. In the region of $_{71}$Lu and $_{73}$Ta isotopes one of the most striking phenomena observed is the behavior of the signature splitting in the bands built on the $\Omega=9/2$ $\pi h_{11/2}$ orbital: (i) in the odd-Z even-N isotopes these bands show unexpectedly large signature splitting, whose amplitude increases considerably with decreasing N down to $N\sim90$ [2–12]. However, after the first backbending (known to be caused by the rotational alignment of a pair of $i_{13/2}$ neutrons) the signature splitting becomes small and signature inversion is observed in several cases. (ii) In odd-odd isotopes the bands built on the $\pi h_{11/2}\otimes\nu i_{13/2}$ configuration show small anomalous signature splitting at low spins (unfavored signature $\alpha=1$ lies at lower excitation energy than the favored signature $\alpha=0$). The signature staggering amplitude increases with decreasing N, and consequently the signature inversion point moves to higher spins (see, for instance, Ref. [13]).

Attempts to reproduce this phenomenon have been made by taking into account the possible deviation from an axially symmetric nuclear shape. Potential energy surface (PES) calculations [14] have shown that a $\pi h_{11/2}$ orbital in the upper half of the shell drives the prolate deformed nucleus towards negative γ deformations ($\gamma\sim-20°$), where the two signatures of the orbital show considerable splitting even at low rotational frequency. On the other hand, the low-Ω components of the $\nu i_{13/2}$ shell strongly favor shapes with $\gamma\gtrsim0$. Therefore if one assumes that the nucleus is sufficiently γ soft to respond to the deformation-driving effect of the odd quasiparticle, then the experimentally observed features of signature splitting in odd-A nuclei and signature inversion in odd-odd nuclei can be qualitatively explained [14].

In the rare-earth region Bengtsson *et al.* [15] have considered the $N\sim90$ and $62<Z<70$ nuclei as sufficiently γ soft for the odd quasiprotons in the $h_{11/2}$ shell to induce a negative γ deformation for which the signature splitting phenomenon can take place. Such phenomena, however, have been experimentally observed up to the $_{73}$Ta isotopes.

This work extends the study of the nuclei in this region with the spectroscopy of the most neutron-deficient tantalum nucleus investigated to date, ^{165}Ta. Although several γ-ray transitions had been identified with ^{165}Ta prior to this work, they had not been assigned to a definitive level scheme [16–18]. The present work establishes the yrast band of ^{165}Ta up to a spin of $53/2^-$. The assignment of the $[514]9/2^-$ configuration to this band is discussed. The observed alignments, bandcrossing frequencies, signature splitting, and $B(M1)/B(E2)$ ratios are compared with results from cranked shell model calculations, and their implications for the nuclear shape are discussed.

II. EXPERIMENTS

High-spin states in ^{165}Ta were populated in two independent reactions using the $K=200$ separated sector cyclotron facility of the National Accelerator Center (NAC) near Cape Town. In the first experiment the reaction ^{142}Nd(^{27}Al,4n)^{165}Ta was investigated at an incident energy of 150 MeV, using a self-supporting ^{142}Nd target foil of thickness 750 μg cm^{-2} enriched to 98.7%. At this energy, the dominant residuals were found to be ^{164}Hf (37%), ^{164}Ta (22%), ^{165}Hf (17%), ^{165}Ta (17%), and

*Present address: Department of Physics, University of Calicut, Calicut 673 635, India.

†Present address: c/o DSpace, Innovation House, First Ave., Technology Park, Mawson Lakes, SA5095, Australia.

‡Present address: Kernfysisch Versneller Instituut, Zernikalaan 25, 9747 AA Groningen, The Netherlands.

^{162}Lu (8%). The figures in parentheses represent the approximate percentage of the total production cross section for the respective channel.

Gamma-gamma coincidences were measured with the AFRODITE γ-ray spectrometer comprising eight Compton-suppressed germanium Clover detectors (two at 45°, four at 90°, and two at 135° relative to the beam direction) and seven fourfold segmented low energy photon spectrometers (LEPS's) (two at 45°, three at 90°, and two at 135° relative to the beam direction). A description of AFRODITE and its performance characteristics can be found in Ref. [19]. The event trigger condition required a three-or-higher-fold coincidence between any of the 15 detectors. With these conditions a data set of 538 million coincident events was acquired during some 206 hours of beam time.

In the off-line analysis, the raw event data from all detectors were calibrated using standard ^{133}Ba and ^{152}Eu sources and Doppler corrected using an empirically determined β value ($\beta \simeq 0.0153$). The Clover data were sorted into symmetric $E_\gamma - E_\gamma$ as well as asymmetric matrices for a determination of γ-ray multipolarities based on the directional correlation of decays from oriented states (DCO) method [20]. Both LEPS and Clover data were also used to construct a three dimensional $E_\gamma - E_\gamma - E_\gamma$ cube. Analysis of the coincidence relationships was carried out using standard RADWARE software [21].

In the second experiment high-spin states of ^{165}Ta were populated in the reaction ^{141}Pr(^{28}Si,4n)^{165}Ta at an incident energy of 142 MeV, using a thick 17-mg cm^{-2} target. The most important residual nuclei were determined to be ^{166}Ta (41%), ^{166}Hf (23%), ^{165}Ta (19%), ^{165}Hf (14%), and ^{164}Hf (2%). Except for ^{165}Ta level schemes for all of the above have been identified [22,23]. Gamma-gamma coincidences were detected using AFRODITE with seven Clovers and eight LEPS's. In all other important respects the setup for both experiments was identical. A data set of 106 million three-and-higher-fold coincidences was acquired during about 50 hours of beam time, and the raw event data sorted into matrices for subsequent analysis.

III. LEVEL SCHEME

The yrast rotational decay sequence of ^{165}Ta presented in Fig. 1, up to spin 53/2 at an excitation energy of 6168 keV, is based on the present work. Gamma rays from ^{165}Ta had been previously identified by Clark *et al.* [16] but to our knowledge no definitive decay scheme has yet been constructed. Preliminary calculations of reaction cross sections using the EVAPOR code [24] predicted that both the ^{164}Ta and ^{165}Ta channels would be strongly populated in the first experiment, while the second experiment was expected to produce mainly ^{165}Ta and ^{166}Ta, but no ^{164}Ta. At the present time the decay scheme of ^{164}Ta is also unknown. Consequently the γ rays assigned to ^{164,165}Ta in the first experiment, by gating on the Ta x rays, could not be unambiguously identified with either ^{164}Ta or ^{165}Ta. We therefore compared their production yield with that in the second experiment. Since the high-spin structure of ^{166}Ta is known [22], γ rays present in both data sets, which are also in coincidence with the Ta x rays, were assigned to ^{165}Ta.

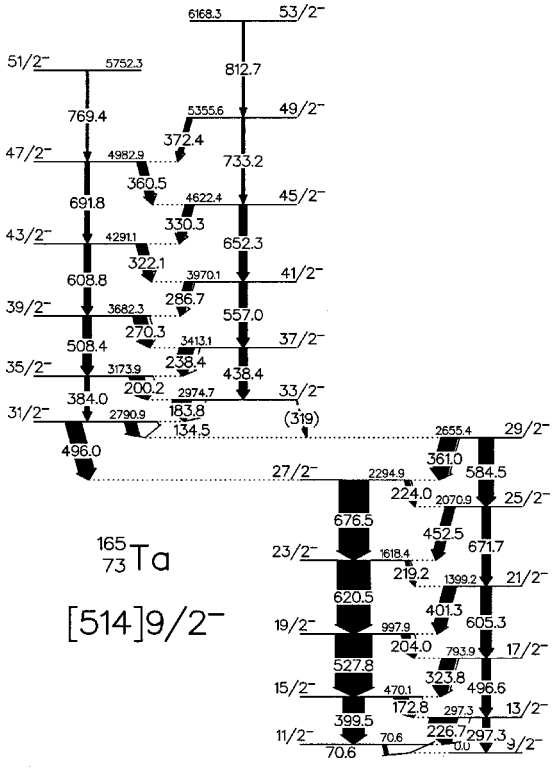

FIG. 1. Level scheme of the yrast band of ^{165}Ta. The widths of the arrows indicate the transitions intensities. Excitation energies are relative to the 9/2$^-$ level energy (assumed 0 keV).

For instance, the transition 134.5 keV was found to belong to a band sequence that is in coincidence with the Ta x rays in both sets of experimental data. Figure 2(a) shows the spectrum obtained from the ^{142}Nd(^{27}Al,4n)^{165}Ta reaction data in coincidence with the 134.5-keV transition. This is to be compared with the spectrum obtained by setting a gate on the 134.5-keV γ ray, but using the E_γ-E_γ matrix constructed from the ^{141}Pr(^{28}Si,4n)^{165}Ta reaction data, in Fig. 2(b). Since the γ rays in this gate are not from ^{166}Ta [22], and

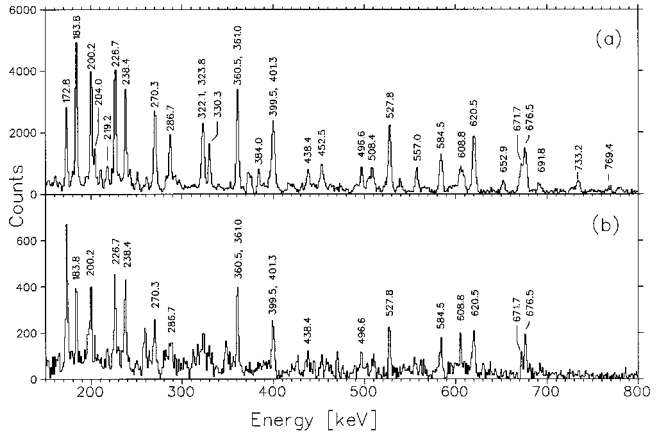

FIG. 2. Coincidence spectra gated on the 134.5-keV transition in Ta, measured in the reactions (a) ^{142}Nd(^{27}Al,4n)^{165}Ta and (b) ^{141}Pr(^{28}Si,4n)^{165}Ta.

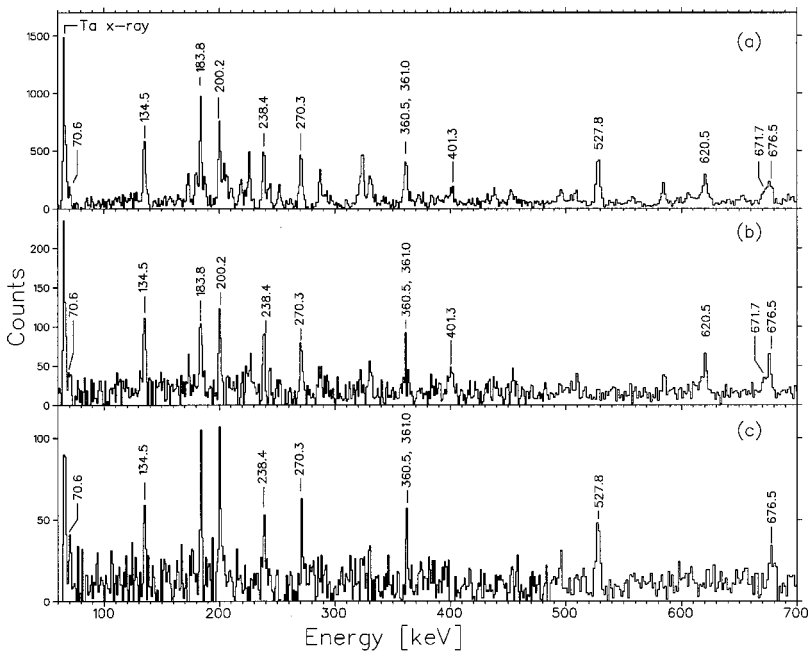

FIG. 3. Selected triple coincidence spectra. (a) Double gate on 399.5 keV and the Ta x ray. (b) Double gate on 399.5 and 527.8 keV. (c) Double gate on 399.5 and 620.5 keV.

since ^{164}Ta was not expected among the residuals in the second experiment, they were assigned to ^{165}Ta. This conclusion is supported by a previous identification of a number of these transitions with ^{165}Ta on the basis of mass 165 recoils [17,18].

The level scheme was constructed on the basis of γ-ray coincidence relationships and intensities. The analysis of triple coincidences obtained by setting double gates on the cube proved essential in resolving multiplets and placing them in the level scheme. For example, an unresolved doublet of about 400 keV occurs in the band. The spectrum in coincidence with the 399.5-keV transition and the Ta x ray shows a strong line at 401.3 keV in addition to the other strong transitions in the band [Fig. 3(a)]. The 401.3-keV transition is still visible in the spectrum double gated on the 399.5 and 527.8-keV γ rays, seen in Fig. 3(b), but is absent from the spectrum double gated on 399.5 and 620.5 keV presented in Fig. 3(c). We have therefore placed the 401.3-keV transition parallel to 620.5 keV. In a similar way the remaining doublets of 323, 361, and 496 keV could be placed into the level scheme. Strong doublets were also seen at 173 and 226 keV. However, an analysis of double-gated spectra revealed that these transitions are both singlets in this band, whereas they occur as doublets in a different band. In addition a number of other transitions (179, 188, 207, 210, 225, 251, 252 keV) have been identified as belonging to a different decay sequence in ^{165}Ta, but it has not been possible to place these in a consistent level scheme at the present time. We have not been able to identify transitions depopulating the lowest lying levels of the yrast band. This can be due to the very low energy of the decaying transitions or long lifetimes.

It is known that the bands of odd nuclei in this mass region typically comprise two signature partner sequences, linked via cascade transitions. The level scheme for ^{165}Ta deduced in the present work is consistent with this trend. The directional correlation ratios [DCO ratios $I_\gamma(45°)/I_\gamma(90°)$] for these cascade transitions in the level scheme are close to 0.8, while DCO ratios for the in-band crossover transitions are close to 1.3. These values are consistent with dipole and quadrupole transitions, respectively. The assignment of either electric or magnetic character to the 20 strongest transitions in the band is supported without exception by linear polarization measurements performed using the Clovers as polarimeters as described in Ref. [25]. The experimental anisotropies A for transitions in the yrast band were calculated from the expression

$$A=\frac{N_V-\alpha N_H}{N_V+\alpha N_H}$$

with relative efficiency $\alpha=0.994$, where N_V denotes the number of γ rays which scattered in a plane perpendicular to the beam axis, and N_H the number which scattered in a plane parallel to the beam axis. The sign of A is positive for stretched electric transitions, and negative for stretched magnetic transitions. On the basis of the anisotropies and DCO measurements, most transitions could be assigned $M1$ or $E2$ character. The DCO ratio value for the 400-keV doublet is intermediate between the values for a dipole and a quadrupole transition, consistent with the placement of the 399.5 ($E2$) and 401.3 keV ($M1$) transitions in the level scheme.

The γ-ray intensities for clean transitions were determined from the coincidence projection of a gate set on the Ta x rays. It was verified that the relative intensities of these transitions to other transitions in the band were not skewed by gating on the x ray. For the remaining transitions, the intensities were determined by using the $E_\gamma-E_\gamma-E_\gamma$ cube to generate double-gated spectra. In the upper part of the band, above the $29/2^-$ level, most of the intensity is carried by $M1$ transitions. Below the $27/2^-$ level, however, most of the gamma intensity flows through the favored $\alpha=-1/2$ sequence of $E2$ transitions.

TABLE I. Level energies, spin assignments, γ-ray transition energies, intensities, branching ratios, $B(M1)/B(E2)$, DCO ratios, and the anisotropy in ^{165}Ta.

E_{ex} (keV)[a]	Initial→ final spin	E_γ (keV)[b]	I_γ [c]	Branching ratio[d]	$B(M1)/B(E2)$[e]	DCO ratio $\frac{I_\gamma(45°)}{I_\gamma(90°)}$	A $\frac{N_V-\alpha N_H}{N_V+\alpha N_H}$ [h]
70.6	$\frac{11}{2}^- \rightarrow \frac{9}{2}^-$	70.6	206(43)			1.01(20)	[f]
297.3	$\frac{13}{2}^- \rightarrow \frac{9}{2}^-$	297.3	181(80)	0.12(06)	1.16(54)	[f]	[f]
	$\frac{13}{2}^- \rightarrow \frac{11}{2}^-$	226.7	1506(211)			1.06(15)[g]	−0.08(1)
470.1	$\frac{15}{2}^- \rightarrow \frac{11}{2}^-$	399.5	1133(226)	1.43(40)	0.96(26)	1.02(14)[g]	+0.07(1)
	$\frac{15}{2}^- \rightarrow \frac{13}{2}^-$	172.8	790(150)			0.90(13)	−0.14(2)
793.9	$\frac{17}{2}^- \rightarrow \frac{13}{2}^-$	496.6	456(46)	0.58(15)	1.07(28)	1.54(30)[g]	+0.06(1)[g]
	$\frac{17}{2}^- \rightarrow \frac{15}{2}^-$	323.8	787(189)			0.80(15)[g]	−0.10(1)
997.9	$\frac{19}{2}^- \rightarrow \frac{15}{2}^-$	527.8	1978(59)	4.33(62)	0.78(11)	1.16(19)	+0.07(1)
	$\frac{19}{2}^- \rightarrow \frac{17}{2}^-$	204.0	457(64)			0.68(19)	[f]
1399.2	$\frac{21}{2}^- \rightarrow \frac{17}{2}^-$	605.3	572(132)	0.91(29)	0.96(31)	[f]	[f]
	$\frac{21}{2}^- \rightarrow \frac{19}{2}^-$	401.3	626(138)			1.02(14)[g]	−0.07(1)
1618.4	$\frac{23}{2}^- \rightarrow \frac{19}{2}^-$	620.5	1790(54)	8.91(93)	0.68(07)	1.28(20)	+0.07(1)
	$\frac{23}{2}^- \rightarrow \frac{21}{2}^-$	219.2	201(20)			0.62(10)	[f]
2070.9	$\frac{25}{2}^- \rightarrow \frac{21}{2}^-$	671.7	437(136)	0.88(30)	1.18(40)	[f]	[f]
	$\frac{25}{2}^- \rightarrow \frac{23}{2}^-$	452.5	499(65)			0.84(17)	−0.05(1)
2294.9	$\frac{27}{2}^- \rightarrow \frac{23}{2}^-$	676.5	1606(209)	6.35(101)	1.38(22)	1.25(17)	+0.06(1)
	$\frac{27}{2}^- \rightarrow \frac{25}{2}^-$	224.0	253(23)			[f]	[f]
2655.4	$\frac{29}{2}^- \rightarrow \frac{25}{2}^-$	584.5	775(109)	0.87(24)	1.16(32)	1.49(30)	+0.03(1)
	$\frac{29}{2}^- \rightarrow \frac{27}{2}^-$	361.0	890(214)			0.84(12)[g]	−0.11(1)
2790.9	$\frac{31}{2}^- \rightarrow \frac{27}{2}^-$	496.0	862(78)	1.39(17)	6.18(75)	1.54(30)[g]	+0.06(1)
	$\frac{31}{2}^- \rightarrow \frac{29}{2}^-$	134.5	619(50)			0.85(12)	[f]
2974.7	$\frac{33}{2}^- \rightarrow \frac{29}{2}^-$	(319)	$\leqslant$40	$\leqslant$0.04	$\geqslant$12.1	[f]	[f]
	$\frac{33}{2}^- \rightarrow \frac{31}{2}^-$	183.8	1000(80)			0.78(11)	−0.15(3)
3173.9	$\frac{35}{2}^- \rightarrow \frac{31}{2}^-$	384.0	229(41)	0.29(06)	2.54(50)	[f]	[f]
	$\frac{35}{2}^- \rightarrow \frac{33}{2}^-$	200.2	801(64)			0.83(12)	−0.22(3)
3413.1	$\frac{37}{2}^- \rightarrow \frac{33}{2}^-$	438.4	449(86)	0.55(11)	1.51(29)	[f]	+0.11(1)
	$\frac{37}{2}^- \rightarrow \frac{35}{2}^-$	238.4	813(24)			0.89(12)	−0.09(1)
3682.3	$\frac{39}{2}^- \rightarrow \frac{35}{2}^-$	508.4	452(162)	0.62(23)	1.93(70)	[f]	+0.08(1)
	$\frac{39}{2}^- \rightarrow \frac{37}{2}^-$	270.3	727(51)			0.78(11)	−0.09(1)
3970.1	$\frac{41}{2}^- \rightarrow \frac{37}{2}^-$	557.0	454(64)	0.82(12)	1.93(28)	0.93(38)	+0.18(1)
	$\frac{41}{2}^- \rightarrow \frac{39}{2}^-$	286.7	551(220)			0.81(11)	−0.08(1)
4291.1	$\frac{43}{2}^- \rightarrow \frac{39}{2}^-$	608.8	338(68)	0.71(21)	2.45(72)	[f]	[f]
	$\frac{43}{2}^- \rightarrow \frac{41}{2}^-$	322.1	475(101)			0.80(15)[g]	−0.10(1)
4622.4	$\frac{45}{2}^- \rightarrow \frac{41}{2}^-$	652.3	421(59)	1.01(15)	2.27(35)	1.25(25)	+0.11(2)
	$\frac{45}{2}^- \rightarrow \frac{43}{2}^-$	330.3	418(25)			0.78(12)	−0.18(1)
4982.9	$\frac{47}{2}^- \rightarrow \frac{43}{2}^-$	691.8	228(93)	0.53(24)	4.45(202)	[f]	+0.07(1)
	$\frac{47}{2}^- \rightarrow \frac{45}{2}^-$	360.5	430(86)			0.84(12)[g]	−0.11(1)

TABLE I. (*Continued*.)

E_{ex} (keV)[a]	Initial→ final spin	E_γ (keV)[b]	I_γ [c]	Branching ratio[d]	$B(M1)/B(E2)$[e]	DCO ratio $\frac{I_\gamma(45°)}{I_\gamma(90°)}$	A $\frac{N_V-\alpha N_H}{N_V+\alpha N_H}$ [h]
5355.6	$\frac{49}{2}^- \rightarrow \frac{45}{2}^-$	733.2	167(43)	0.64(18)	4.47(123)	1.50(30)	[f]
	$\frac{49}{2}^- \rightarrow \frac{47}{2}^-$	372.4	261(25)			[f]	[f]
5752.3	$\frac{51}{2}^- \rightarrow \frac{47}{2}^-$	769.4	122(20)			[f]	[f]
6168.3	$\frac{53}{2}^- \rightarrow \frac{49}{2}^-$	812.7	129(30)			[f]	[f]

[a]Relative to the $\frac{9}{2}^-$ level.
[b]Uncertainties: 0.3 keV, but up to 1.0 keV for weak transitions and multiple lines.
[c]Normalized to the 183.8-keV $\frac{33}{2}^- \rightarrow \frac{31}{2}^-$ transition. Uncertainties: 5–10 % for weak transitions, and up to 50% for multiple lines.
[d]$\lambda = I_\gamma(I \rightarrow I-2)/I_\gamma(I \rightarrow I-1)$.
[e]Determined assuming $\delta^2 = 0$.
[f]Could not be determined due to poor statistics.
[g]Unresolved doublet. DCO ratio is for total peak.
[h]$\alpha = 0.994$.

From our data it was not possible to firmly establish the existence of a 319-keV transition between the $33/2^-$ and $29/2^-$ levels. The placement of this transition in the level scheme is therefore tentative. An upper limit for the branching ratio of the decay out of the $33/2^-$ level was found to be $I_\gamma(319)/I_\gamma(183.8) \leqslant 0.04$. The level energies, γ-ray energies, intensities, spin assignments, DCO ratios, and anisotropies are summarized in Table I.

In order to look for isomeric states (nanosecond range), the recoil shadow anisotropy method (RSAM) [26], that requires no additional device besides the AFRODITE array, was used. We did not find any evidence for isomers in the nanosecond range in ^{165}Ta.

Because no low-spin states in ^{165}Ta had been identified prior to this work, and because no transitions deexciting the lowest-lying levels of the yrast band were observed, the spin and parity of the band head could not be measured experimentally. They were therefore assigned on the basis of systematics. This method has been used for bands in several of the heavier odd-mass Ta isotopes [2–4,27–29]. The lowest-lying level of the yrast band was assigned a spin and parity of $9/2^-$ and configuration $[514]9/2^-$ based on the following arguments:

(i) Excitation energies of the yrast states relative to the lowest-lying level observed in ^{165}Ta were compared with relative excitation energies in bands built on different intrinsic configurations for the heavier odd-mass $^{167\text{-}179}$Ta isotopes [2–4,27–30]. Our data follow the smooth trend of the level excitation energies only for bands assigned to the $[514]9/2^-$ orbital, and only if it is assumed that the spin and parity of the lowest-lying observed level is $9/2^-$ (see Fig. 4).

(ii) A large signature splitting (69 keV at $\hbar\omega = 0.225$ MeV) of the yrast band below the backbend was measured. Since this is a characteristic feature only for bands built on the negative parity $\pi h_{11/2}$ orbital in the lighter odd-Z even-N rare earths with $N \leqslant 94$ (e.g., ^{159,161,163,165}Lu, see for example, Ref. [6], ^{167}Ta [2]), the $\pi h_{11/2}$ orbital should be associated with this band.

(iii) Figure 5 shows the systematic variation of the energy staggering amplitude $E(I)-E(I-1)$ as a function of spin for the $\pi h_{11/2}[514]9/2^-$ bands of the odd-A $^{165-179}$Ta isotopes. The ^{165}Ta yrast band follows the observed trend, with favored states lying lower in energy than unfavored states and a sudden decrease in the staggering amplitude at $I = 29/2$, only if spin 9/2 is assigned to the lowest level of the yrast band.

(iv) Among the available negative parity, high-Ω proton orbitals for the odd-A isotopes $^{167\text{-}185}$Ta, the $\pi[514]9/2^-$ orbital was calculated to be the closest to the Fermi surface [1]. Our CSM calculations suggest that this will also be true for ^{165}Ta (see Sec. IV). Indeed, the strongly coupled bands assigned to this configuration in the neighboring odd-mass Ta isotopes have been found to lie at relatively low excitation energy, with the trend to become yrast for lighter isotopes (as it is for ^{167}Ta [2]).

(v) The measured $B(M1)/B(E2)$ ratios (see Sec. IV) for the ^{165}Ta yrast band are consistent with the assignment of the $[514]9/2^-$ intrinsic configuration to this band.

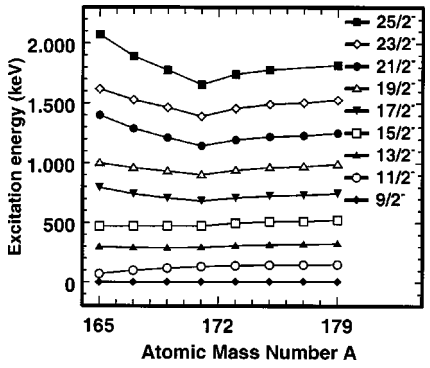

FIG. 4. Excitation energies in the bands built on the $[514]9/2^-$ orbital. The energies are relative to the $9/2^-$ level energies in $^{165-179}$Ta nuclei.

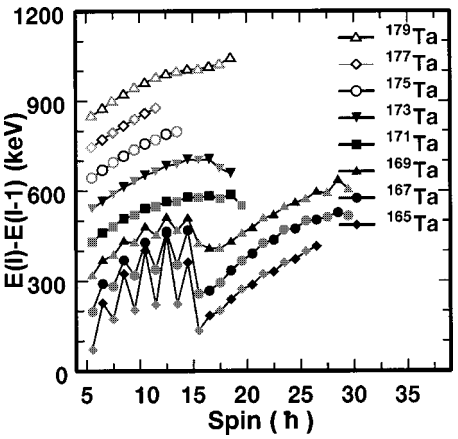

FIG. 5. The systematics of the energy difference $E(I)-E(I-1)$ in the bands built on the $[514]9/2^-$ orbital for the $^{165-179}$Ta nuclei. To avoid superposition of data corresponding to different isotopes, they are succesively offset by 100 keV. The black (grey) symbols correspond to the unfavored (favored) signature of the $[514]9/2^-$ orbital.

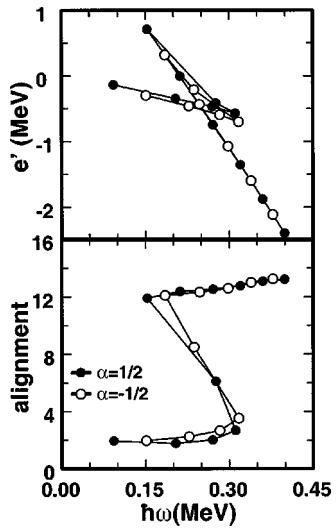

FIG. 6. Upper panel: the experimental Routhians for the $[514]9/2^-$ band in ^{165}Ta. Lower panel: the experimental alignment for the $[514]9/2^-$ band in ^{165}Ta. A core reference with $J_0=21\ \hbar^2\ \mathrm{MeV}^{-1}$ and $J_1=63\ \hbar^4\ \mathrm{MeV}^{-3}$ has been used.

IV. DISCUSSION

A. Experimental quantities in the rotating frame

1. Experimental Routhians, alignments, and band crossings

In order to study the rotational motion of a deformed nucleus, it is convenient to transform the experimental excitation energies and spins into the rotating frame [31]. The degree of rotational alignment $i(\omega)$ can be expressed by

$$i(\omega)=I_x(\omega)-I_{ref}, \tag{1}$$

where $I_x(\omega)$ is the component of total angular momentum of the band on the axis of rotation and I_{ref} is the total aligned angular momentum of a reference configuration, and

$$I_{ref}=\omega J_o+\omega^3 J_1, \tag{2}$$

$$I_x(I)=\sqrt{\left(I+\frac{1}{2}\right)^2-K^2}, \tag{3}$$

$$\omega(I)=\frac{E_f-E_i}{I_x(I_f)-I_x(I_i)}, \tag{4}$$

where J_o and J_1 are the Harris parameters of the rotational reference configuration. The parameters $J_o=21\ \hbar^2\ \mathrm{MeV}^{-1}$ and $J_1=63\ \hbar^4\ \mathrm{MeV}^{-3}$ corresponding to the even-even ^{164}Hf core [23] were used in our calculations.

The experimental level energies $E(I)$ are transformed from the laboratory frame to the rotating frame E^ω according to [31]

$$E^\omega=E(I)-\hbar\omega I_x. \tag{5}$$

The Routhian is obtained by subtracting a reference $E_{ref}=-(\omega^2/2)J_o-(\omega^4/4)J_1+(1/8J_o)$ from E^ω. From the plot of experimentally determined Routhians and alignments (Fig. 6) for both signatures of the yrast band one can measure the experimental crossing frequencies: $\hbar\omega=0.26$ MeV for the negative signature sequence and $\hbar\omega=0.25$ MeV for the positive signature sequence, with an alignment gain of $\approx 10\hbar$.

2. Signature splitting

Signature α is the quantum number associated with the rotation operator: $R_x(\pi)\psi=e^{-i\pi j_x}\psi=e^{-i\pi\alpha}\psi$. A symmetry of the nuclear wave function with respect to $R_x(\pi)$ relates states separated by $\Delta I=2$. In an odd nucleus, the signature defined by $\alpha_f=\frac{1}{2}(-1)^{j-1/2}$ (favored signature) is lowered with respect to the $\alpha_u=\frac{1}{2}(-1)^{j+1/2}$ (unfavored) signature [32], where the angular momentum of the odd particle is expressed by j. The rotational sequence presented in Fig. 1 shows a lowering of the favored $\alpha=-\frac{1}{2}$ sequence with respect to the unfavored one corresponding to $\alpha=+\frac{1}{2}$.

The experimental signature splitting $\Delta e'$, i.e., the difference in energy at a given frequency between the unfavored and favored signatures for the yrast band can be seen in Fig. 6. The signature splitting is of the order of 69 keV below the band crossing, and reverses and is much smaller after the band crossing.

3. Electromagnetic transition probabilities

From the γ-ray intensities in Table I we obtained the branching ratios $\lambda=[I_\gamma(E2)]/[I_\gamma(M1)]$. The ratios of the reduced transition probabilities can be determined using the expression

$$\frac{B(M1,I\rightarrow I-1)}{B(E2,I\rightarrow I-2)}=0.697\cdot\frac{E_\gamma^5(E2)}{E_\gamma^3(M1)}\cdot\frac{1}{\lambda(1+\delta^2)}\quad[\mu^2/e^2\mathrm{b}^2]. \tag{6}$$

The mixing ratios $\delta^2=I_\gamma(E2,I\rightarrow I-1)/I_\gamma(M1,I\rightarrow I-1)$ could not be evaluated in our case (lack of angular correlation data). The δ^2 values estimated from a rotational formula

TABLE II. Convention for labeling the orbitals described by different parity and signature quantum numbers. The neutron (proton) configurations are described by uppercase (lowercase) letters.

Shell model label	Nilsson label	(π,α)	Adopted label
$\pi h_{11/2}$	$[514]9/2^-$	$(-,-\frac{1}{2})$	e
$\pi h_{11/2}$	$[514]9/2^-$	$(-,+\frac{1}{2})$	f
$\nu i_{13/2}$	$[651]3/2^+$	$(+,+\frac{1}{2})$	A
$\nu i_{13/2}$	$[651]3/2^+$	$(+,-\frac{1}{2})$	B

(e.g., Ref. [33]) are found to be small. Therefore we have assumed $\delta=0$ in this analysis. The error introduced by this assumption is negligible compared with the errors in λ.

The branching ratios λ and the $B(M1)/B(E2)$ ratios determined for the yrast band are listed in Table I. At low spins the ratio shows a signature dependence. An increase in the $B(M1)/B(E2)$ ratios is observed at the $\nu i_{13/2}$ crossing, signaling a change in the nature of the wave functions.

B. Calculations

1. Total Routhian surface calculations

Total Routhian surface (TRS) calculations [34] were performed to give an indication of nuclear deformations for various configurations. The calculations were based on the cranked shell model, employing the universal Woods-Saxon potential [35] and the Strutinsky shell-correction formalism. They predict the nuclear shape [parametrized in terms of the quadrupole (β_2), and hexadecapole (β_4) degrees of freedom including a nonaxial deformation (γ)], by minimizing the total Routhian with respect to the shape parameters $\hat{\beta}=(\beta_2,\beta_4,\gamma)$ for different configurations and as a function of the rotational frequency. The Lund convention for γ [36] is used. More details regarding the general method used, can be found in Refs. [34,37,38].

Calculations of TRSs were performed for a number of low lying one-quasiproton configurations. Since at high rotational frequencies signature $\alpha(I=\alpha \bmod 2)$ and parity π are the only two good quantum numbers, the quasiparticle configurations were labeled using the convention described in Table II. One should keep in mind that the Nilsson labels associated with each configuration are strictly valid only at $\hbar\omega=0$ MeV, while the shell model labels are approximately valid only at small quadrupole deformations. The TRS minima for the lowest negative parity one-quasiproton configurations e and f are given in Table III. Each TRS has a well defined parity and signature but no other conserved quantum numbers. Different parts of one surface may therefore correspond to different configurations.

TABLE III. Equilibrium deformations of the lowest quasiproton configurations obtained from the TRS calculations at $\hbar\omega=0.150$ MeV, corresponding to ^{165}Ta.

$(\pi,\alpha)_p$	Label	β_2	γ	β_4
$(-,+\frac{1}{2})$	f	0.176	−0.2	0.006
$(-,-\frac{1}{2})$	e	0.177	−0.8	0.006

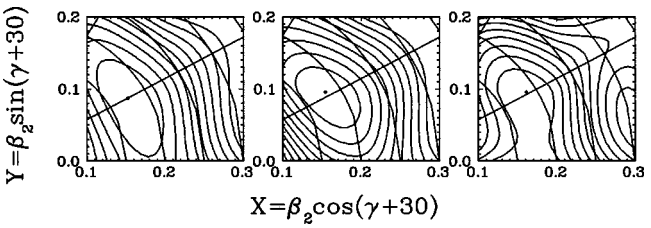

FIG. 7. Total Routhian surfaces calculated for configuration $(\pi,\alpha)=(-,-1/2)$ before and after the $\nu i_{13/2}$ alignment. The left figure corresponds to $\hbar\omega=0.15$ MeV (minimum at $I=4.6\hbar$, $\beta_2=0.177$, $\gamma=-0.8$, $\beta_4=0.006$), the middle figure to $\hbar\omega=0.25$ MeV (minimum at $I=17.6\hbar$, $\beta_2=0.180$, $\gamma=1.0$, $\beta_4=0.017$), while the right figure corresponds to $\hbar\omega=0.40$ MeV (minimum at $I=25.1\hbar$, $\beta_2=0.185$, $\gamma=+0.2$, $\beta_4=0.015$).

Selected examples of TRSs for the lowest-lying $(\pi,\alpha)=(-,-1/2)$ configuration before and after the neutron alignment are presented in Fig. 7. The calculated surface of this negative parity configuration is γ soft at low rotational frequencies: the lowest energy contour line, corresponding to an energy difference of 100 keV, includes γ values varying from $-20°$ to $+20°$, with potential energy minimum at prolate deformation with $\beta_2\sim0.18$ (left panel in Fig. 7). After the first band crossing no significant changes are predicted for the nuclear shape, it is still γ soft with the energy minimum at about the same quadrupole deformation with small γ deformation (middle panel in the same figure). At still higher rotational frequencies, in addition to the minimum at ''normal'' deformation, other potential energy minima appear corresponding to much larger quadrupole deformation. This is not unexpected, since in the neighboring ^{163}Lu and ^{165}Lu nuclei such highly deformed shapes were both theoretically predicted and experimentally observed [9,39]. In ^{165}Ta, however, although such shape coexistence is predicted already at $\hbar\omega\sim0.40$ MeV and $I\simeq24\hbar$ (see the right panel in Fig. 7), it has not been observed in our data.

2. Single-particle energies and cranked shell model calculations

The single-particle proton and neutron levels calculated with a Woods-Saxon potential[1] for $Z=73$ and $N=92$ are presented in Fig. 8. For the predicted nuclear deformation of $\beta_2\sim0.18$, the single particle orbitals lying close to the $Z=73$ Fermi level are $[404]\frac{7}{2}^+$, $[402]\frac{5}{2}^+$, $[523]\frac{7}{2}^-$, and $[514]\frac{9}{2}^-$ (as shown in Fig. 8).

The quasiparticle Routhians for neutrons and protons (see Ref. [31] for a detailed explanation) are plotted in Fig. 9 as a

[1]The mean field was described by ''universal'' parameters determined by the Warsaw group [40]. A detailed comparison between the modified harmonic oscillator (Nilsson) potential and the Woods-Saxon potentials is provided in Ref. [41]. Note that there are some differences [42], compared to the standard modified harmonic oscillator Nilsson diagrams, in particular, the reordering of the $1g_{7/2}$ and $2d_{5/2}$ shells.

function of the rotational frequency for deformation parameters obtained from the minimum in the TRS ($\beta_2=0.177$, $\beta_4=0.006$, $\gamma=-0.8°$, $\Delta_n=1.06$ MeV, and $\Delta_p=1.11$ MeV). The lowest lying proton orbital, as shown in Fig. 9, is predicted to be $[514]9/2^-$, which was one of the arguments used for the assignment of this configuration to the yrast band of ^{165}Ta. However, the predicted signature splitting between the *e* and *f* Routhians is ~11 keV at $\hbar\omega \sim 0.225$ MeV, much smaller than the experimentally measured value of 69 keV. Since the odd proton occupies the *e* level, the crossing at $\hbar\omega \sim 0.42$ MeV is blocked and the first proton alignment is predicted at $\hbar\omega \sim 0.51$ MeV. For neutrons, at $\hbar\omega \sim 0.20$ MeV the vacuum is crossed by the *AB* configuration and a change in the aligned angular momentum $\Delta i \simeq 11\hbar$ is predicted. The next change in the aligned angular momentum occurs at $\hbar\omega \sim 0.32$ MeV. A comparison with the experimentally measured band crossing frequency and gain in alignment in the yrast band suggests that the first band crossing involves the alignment of an $i_{13/2}$ neutron pair. This suggestion is supported by the systematics, as such a neutron band crossing is systematically observed in all the nuclei in the rare-earth mass region. However, the band crossing frequency $\hbar\omega_c \sim 0.20$ MeV predicted by CSM for the yrast band of ^{165}Ta is rather low in comparison with the experimentally measured $\hbar\omega_c \sim 0.26$ MeV.

The experimental Routhians (Fig. 6, upper panel) for the $[514]9/2^-$ band indicate that the interaction strength between the one-quasiparticle and three-quasiparticle bands is $|V| \sim 100$ keV. This is consistent with the results of CSM calculations (see upper panel of Fig. 9).

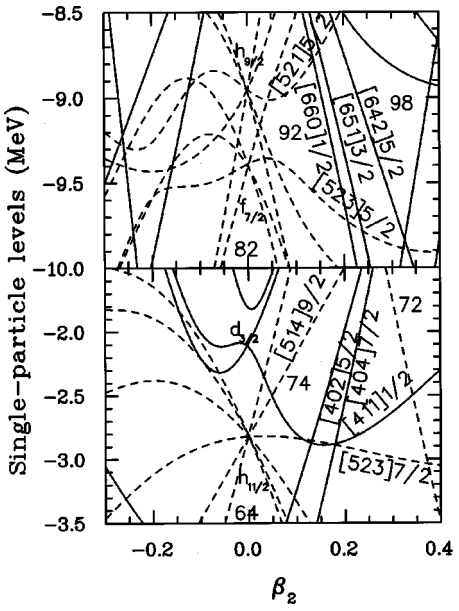

FIG. 8. Single-particle levels calculated with a Woods-Saxon potential appropriate for $N=92$ neutrons (upper panel) and for $Z=73$ protons (lower panel). The orbitals are labeled with the asymptotic quantum numbers $[N,n_z,\Lambda]\Omega$. Positive parity orbitals are represented by the solid lines while the negative parity orbitals are represented by the dashed lines.

3. B(M1)/B(E2) ratios

Some discrepancies were also observed when comparing experimental $B(M1)/B(E2)$ ratios with theoretical predictions, obtained by using a semiclassical approximation based on the cranking approach (e.g., Ref. [43]):

$$\frac{B(M1,I\rightarrow I-1)}{B(E2,I\rightarrow I-2)} = \frac{12}{5Q_o^2\cos^2(30°+\gamma)}\left(1-\frac{K^2}{\left(I-\frac{1}{2}\right)^2}\right)^{-2}\cdot K^2 \times\left[(g_p-g_R)\left(\sqrt{1-\frac{K^2}{I^2}}-\frac{i_p}{I}\pm\frac{\Delta e'}{\hbar\omega}\right)-(g_n-g_R)\frac{i_n}{I}\right]^2, \quad (7)$$

where g_R is the *g* factor of the collective rotation and g_p (g_n) the intrinsic *g* factor of the quasiproton (quasineutron). The proton and neutron aligned angular momenta are denoted by i_p and i_n, and $\Delta e'$ represents the experimental signature splitting. The formula is valid only for axially symmetric nuclei but can be expected to give a reasonable description for ^{165}Ta if only a small deviation from axial symmetry is assumed.

A quadrupole moment of $Q_o=4.9\ e$b (calculated as in Ref. [44]) and $\gamma=0°$, reflecting the minimum in the TRS, were used. In order to obtain the average values of the $B(M1)/B(E2)$ ratio the signature splitting was neglected. The gyromagnetic factor g_R was chosen to be 0.4 [45] below the band crossing. Unsatisfactory agreement between the experimental and the theoretical (dash-dotted curve in Fig. 10) values is obtained if we assume $g_p=1.3$. Values between 1.24 and 1.34 were previously used for the *g* factor of the proton $[514]9/2^-$ orbital in ^{167,169}Ta and ^{163,165,167}Lu isotopes [2,3,7–9,11].

The signature splitting in the $B(M1)/B(E2)$ ratios below the backbend has been calculated (the dotted curve in Fig. 10) using the experimentally measured signature splitting $\Delta e'$. In order to obtain a good average overlap with the experimental data a value of $g_p=1.1$ was used. It can be seen that the theoretical curve strongly overestimates the splitting amplitude.

The experimental $B(M1)/B(E2)$ ratios show a sudden increase above the band crossing at $\hbar\omega=0.26$ MeV. This is mainly a result of the increase in the $B(M1)$ values, due to the alignment of the $i_{13/2}$ neutrons, and may also reflect a possible change in the nuclear deformation induced by this quasiparticle alignment. The theoretical $B(M1)/B(E2)$ ratios above the backbend (dashed line in Fig. 10) have been calculated using the values for the aligned angular momenta obtained from the experiment (Fig. 6), the value $g_n=-0.2$ (which is characteristic for $i_{13/2}$ neutrons [46]), and $g_R=0.3$ (which takes into account the increased neutron contribution

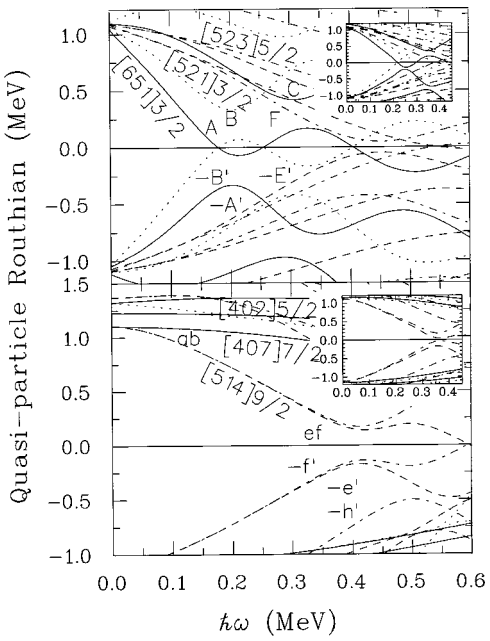

FIG. 9. The quasiparticle Routhians for neutrons (upper panel) and for protons (lower panel) plotted as a function of rotational frequency for ^{165}Ta. The calculations were done using $\beta_2=0.177$, $\gamma=-0.8°$, $\beta_4=0.006$. The insets correspond to calculations using the same parameters, but $\gamma=-18°$. The parity and signature (π,α) of the Routhians are represented as follows: $(+,+1/2)$ solid lines, $(+,-1/2)$ dotted lines, $(-,+1/2)$ dash-dotted lines, and $(-,-1/2)$ dashed lines.

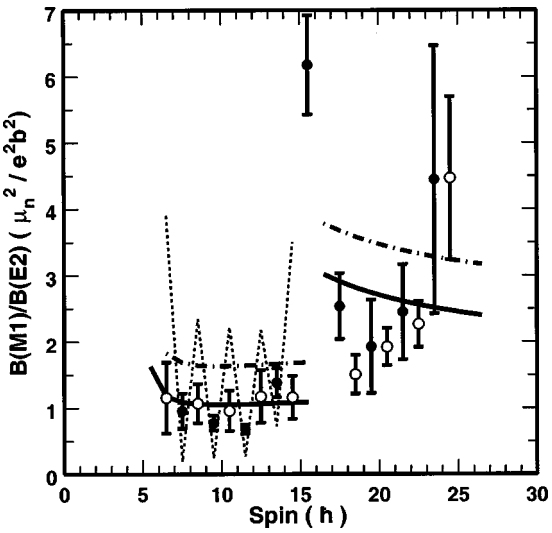

FIG. 10. Ratios of the reduced transition probabilities $B(M1)/B(E2)$ for the $[514]9/2^-$ band in ^{165}Ta obtained from the experiment. The solid (dash-dotted) curve represents the theoretical calculation corresponding to $g_p=1.1$ ($g_p=1.3$), neglecting the signature splitting. The dotted curve represents the theoretical calculation corresponding to $g_p=1.1$, with the experimental signature splitting taken into account (see text for details).

to the moment of inertia). Again unsatisfactory agreement with the experimental ratios was obtained.

The experimental $B(M1)/B(E2)$ data appear to increase smoothly with angular momentum at higher spins. This may reflect a decrease in the $B(E2)$ rates, since the $B(M1)$ rates are not expected to increase (there is no indication of another quasiparticle alignment). For the nuclei ^{156}Dy$_{90}$, ^{160}Yb$_{90}$, and ^{161}Yb$_{91}$ lifetime measurements [47–49] have revealed a decrease in collectivity of the ground band at the $\nu i_{13/2}$ band crossing, which was explained as a result of the decreased nuclear deformation induced by the aligning neutrons. For the more stable ^{166}Yb$_{96}$ lifetime measurements [50] have also shown a loss of collectivity, but at higher spins. In the Lu and Ta isotopes no lifetime measurements have been performed, but in the light ^{161,163,165}Lu isotopes a similar increase in the $B(M1)/B(E2)$ ratio was observed at higher spins [8] and a possible decrease in the nuclear quadrupole deformation was suggested. In the ^{167,169}Ta isotopes no evidence for such increase in the $B(M1)/B(E2)$ has been found [2,3]. Therefore, although it is likely that a decrease in nuclear quadrupole deformation causes the observed increase in the $B(M1)/B(E2)$ ratios at higher spins, lifetime measurements are needed to confirm such a suggestion.

Although the assignment of the $[514]9/2^-$ quasiparticle configuration to the yrast band can be considered unambiguous, the band crossing frequency, the signature splitting of the Routhians and the splitting of the $B(M1)/B(E2)$ ratios, in particular below the backbending, could not be reproduced satisfactorily by the CSM calculations. Indeed, these calculations were made assuming that the nucleus has a rigid deformation described by the parameters at the potential energy minimum of the TRS, while in fact a γ-soft shape was predicted (see Fig. 7).

Similar discrepancies between the experimental quantities and the theoretical CSM predictions were previously found in the neighboring odd-A Ta and Lu nuclei with $N\gtrsim 90$, and were considered as a possible indication of a triaxial and/or γ-soft nuclear deformation [2,5–11]. On the other hand, Bengtsson *et al.* [15] considered that only the rare-earth nuclei with $N\sim 90$ and $62<Z<70$ would be sufficiently γ soft for the odd quasiparticle to drive the nuclear shape toward sizeable γ deformation. Therefore the question about γ deviations from axial symmetry for the light Lu and in particular Ta isotopes remains open.

C. Are the light Ta isotopes nonaxially symmetric?

Although it is difficult to find conclusive experimental evidence [51,52] for the existence of a γ-deformed shape, a number of indications lead to such a suggestion.

1. Increased backbending frequency for N∼90

The upper part of Fig. 11 shows the band crossing frequency $\hbar\omega_c$ of the AB (neutron $i_{13/2}$) alignment for the ground bands in the even-even $_{70}$Yb, $_{72}$Hf, and $_{74}$W isotopes, as well as for the $\pi h_{11/2}$ bands in the odd $_{71}$Lu and $_{73}$Ta isotopes and the $\pi[402]5/2^+$ bands in the odd $_{73}$Ta isotopes, as a function of the neutron number N. The data used in plotting the figures are from Refs. [2–6,12,53–59]. The main trend of the band crossing frequency for the isotopic chains in even-even nuclei is to decrease slowly with decreasing N and then to again increase for the lightest iso-

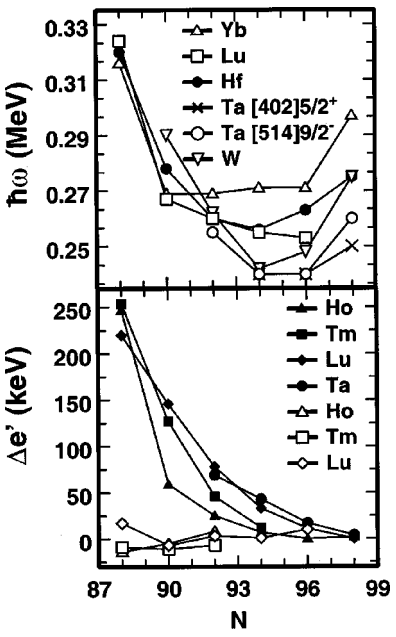

FIG. 11. Upper panel: band crossing frequencies for the $\nu i_{13/2}$ alignment in the ground bands of even-even Yb, Hf, and W isotopes and in the $\pi h_{11/2}$ and $\pi d_{5/2}$ bands in odd Lu and Ta isotopes. Lower panel: signature splitting of the high-Ω $\pi h_{11/2}$ Routhians in the odd rare-earth isotopes with $Z \sim 70$. Filled symbols correspond to the signature splitting below the band crossing measured at $\hbar\omega = 0.225$ MeV, and open symbols to the signature splitting above the band crossing at $\hbar\omega = 0.350$ MeV.

topes. It has been suggested [7,60] that the relative position of the neutron Fermi level with respect to the $\Omega = 1/2$ orbitals of the $i_{13/2}$ shell, as well as the decrease of the monopole pairing energy with increasing N, play a crucial role in explaining this trend. Although this suggestion can qualitatively describe the observed trends, the calculated $\hbar\omega_c$ values lie much lower than the experimental ones for the lightest even-even isotopes [60]. Thus changes in the deformation parameters [60], and in particular deviations from axial symmetry for the $N \gtrsim 88$ isotopes [7], have been proposed.

The AB band crossing frequency in the odd-Z nuclei is similar to that of their even-even neighbors (see Fig. 11). The slightly lower $\hbar\omega_c$ values for the odd-mass isotones have been explained [7] as due to a small decrease in the quadrupole deformation of the nucleus, induced by the odd quasiproton (the positive slopes of the $\pi[514]9/2^-$ and the $\pi[402]5/2^+$ orbitals vs deformation can be seen in Fig. 8). Since for these nuclei the valence protons and neutrons occupy different major shells, the proton-neutron interactions are negligible, and therefore the odd proton is not expected to influence the band crossing frequency [61]. This similarity is therefore an indication that the observed trend in the odd-Z isotopes is mainly due to the properties of the even-even core and will reflect the nuclear shape.

Thus the higher experimental value of $\hbar\omega_c = 0.26$ MeV in $^{165}Ta_{92}$ when compared with the theoretical prediction of 0.20 MeV is very likely a consequence of increased γ softness of the core for this light Ta isotope.

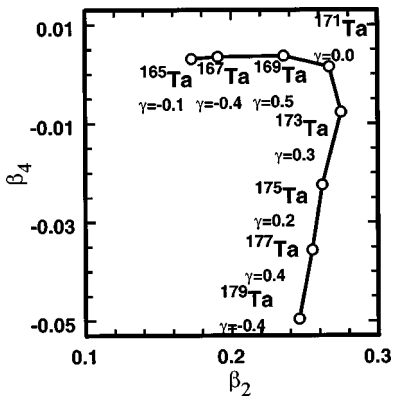

FIG. 12. The β_2 and β_4 deformation parameters for the $^{165-179}$Ta nuclei, calculated by the TRS for the lowest $(-,-1/2)$ proton configuration at $\hbar\omega = 0.131$ MeV.

2. Enhanced signature splitting

The experimentally observed signature splitting in the $9/2^-$ bands in the odd-even rare-earth nuclei is unexpectedly large for the light isotopes, increasing rapidly with decreasing neutron number when approaching the nuclei with $N \sim 90$. The CSM calculations have not been able to reproduce it.

Signature splitting appears as a consequence of the mixing into the wave functions of orbitals with $\Omega = 1/2$, due to the Coriolis interaction. On the other hand, since the proton Fermi level lies high in the $h_{11/2}$ shell the mixing of the $\Omega = 1/2$ components into the wave functions is small for an axially symmetric nuclear shape. Decreasing nuclear quadrupole deformation on the other hand leads to an increased signature splitting since in the lowest order $\Delta e'$ is proportional to $\beta_2^{-2\Omega+1}$ if pairing is neglected [62]. Although an increase in signature splitting is expected with increasing Z and decreasing N (since the quadrupole deformation decreases, see Fig. 12 and Ref. [1]), the predicted magnitude of the splitting is nevertheless much less than observed [5].

Thus, in order to reproduce the large signature splitting of high-Ω orbitals, a mechanism leading to enhanced mixing with an $\Omega = 1/2$ orbital is needed. It seems that for the light odd-mass Ta and Lu isotopes only nonaxially symmetric shapes can cause such an effect.

The enhanced signature splitting in the high-Ω $\pi h_{11/2}$ orbitals observed in the odd-A rare-earth isotopes, has been attributed [14] to deviations from an axially symmetric nuclear shape, since according to the CSM calculations (i) even a 50% change in the pairing gap barely affects the signature splitting; (ii) a variation of quadrupole deformation β_2 within the interval 0.16–0.29 leads to small, almost constant signature splitting of the $\pi h_{11/2}$ orbitals; (iii) the trend of the rapid increase of signature splitting with decreasing neutron number in the bands associated with the same quasiproton configuration strongly suggests a dependence on nuclear shape. In addition, the same authors have shown that the upper-shell $\pi h_{11/2}$ orbitals tend to drive the nuclear shape toward negative γ deformations with $\gamma \sim -20°$, for which a sizable signature splitting of these orbitals is expected. Since the γ softness is predicted to increase with decreasing neu-

tron number toward $N\sim 90$ [15], the largest splittings are expected for these nuclei. It has been also pointed out that the low-Ω orbitals of the neutron $i_{13/2}$ shell strongly drive the nucleus towards $\gamma \gtrsim 0°$. Therefore, after the first backbend, the nuclear shape is expected to be close to axially symmetric, and thus the large signature splitting of the proton $\pi h_{11/2}$ orbitals will disappear. These trends have been experimentally found for all the rare-earth nuclei with $Z<70$, (see, for instance, Refs. [63–65]), as well as for those with $Z\geqslant 70$ (see for instance Refs. [2,6]. The lower part of Fig. 11 shows these trends for a number of isotopes with $Z\sim 70$.

It therefore seems very likely that deviations from an axially symmetric shape play an important role in generating the large signature splitting of the high-Ω $\pi h_{11/2}$ orbitals for the isotones with $N\sim 90$, even for the nuclei with $Z\gtrsim 70$.

3. Overestimated signature splitting in the B(M1)/B(E2) ratios below the backbending

The $B(M1)/B(E2)$ ratios can exhibit a signature splitting, which is known to represent the splitting in the magnetic transition rates $\Delta B(M1)$ [8], where $\Delta B(M1) = B(M1{:}\alpha_f \rightarrow \alpha_u) - B(M1{:}\alpha_u \rightarrow \alpha_f)$. A signature splitting $\Delta e'$ of the Routhians and magnetic rates $\Delta B(M1)$ does not necessarily imply a triaxial nuclear shape, but the magnitude of $\Delta e'$ and $\Delta B(M1)$ can be strongly dependent on γ. In the cranking formalism the relation between magnetic transition rates and $\Delta e'$, as given by Eq. (7), reflects the effect of admixtures of $\Omega = 1/2$ components in the nuclear wave functions. However, this expression is valid only for axially symmetric nuclear shapes.

In the rare-earth region the signature splitting of the $B(M1)/B(E2)$ ratios for the strongly coupled $\pi h_{11/2}$ bands calculated by Eq. (7) often strongly overestimates the experimental value, particularly for the nuclei around $N\sim 90$. Such a result can be considered as a possible sign of deviations of nuclear shape from axial symmetry.

The signature splitting of $B(M1)$ rates can be expressed by the ratio of $\{\Delta[B(M1)/B(E2)]\}/\langle B(M1)/B(E2)\rangle$, where $\langle B(M1)\rangle = \frac{1}{2}[B(M1{:}\alpha_f \rightarrow \alpha_u) + B(M1{:}\alpha_u \rightarrow \alpha_f)]$. This ratio depends neither on the gyromagnetic factors, nor on the $B(E2)$ values since it is believed that the $B(E2)$ values show smooth dependence on spin, and in particular, do not exhibit signature dependence even in the case of triaxially deformed nuclear shapes [66]. Indeed, no signature dependence is found [64] in the measured $B(E2)$ values in ^{157}Ho, which has a pronounced splitting in $B(M1)$ values at low spin in the $\pi h_{11/2}$ $[523]7/2^-$ configuration. Similar results have been reported in ^{159}Tm [67]. The monotonic increase in the deviations between experimental and calculated values of $\Delta B(M1)/\langle B(M1)\rangle$ with decreasing neutron number in Lu isotopes, has been interpreted as a possible consequence of the increased triaxiality and γ softness of the nuclei with N approaching $N\sim 90$ [8]. A similar trend is observed for the ^{165,167}Ta isotopes. The theoretical $\Delta B(M1)/\langle B(M1)\rangle$ ratio is calculated to lie within the experimental error bars for ^{167}Ta, whereas for ^{165}Ta the theoretical is found to exceed the experimental ratio by a factor of about 4.9 as shown in Fig. 13. This is an indication for increased deviation from axial symmetry of the nuclear shape.

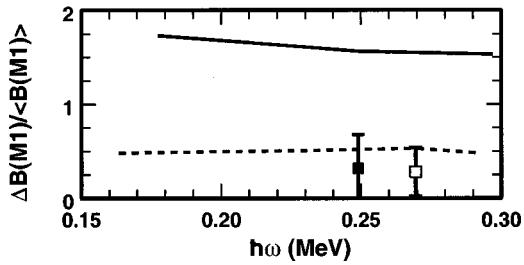

FIG. 13. $\Delta B(M1)/\langle B(M1)\rangle$ ratios shown as a function of rotational frequency for the $[514]9/2^-$ bands. The solid (dotted) line represents the theoretical values in ^{165}Ta (^{167}Ta). Also shown are the experimental values for ^{165}Ta (filled square) and ^{167}Ta (open square) at rotational frequencies of 0.25 and 0.27 MeV, respectively.

A theoretical study of the $\Delta B(M1)/\langle B(M1)\rangle$ ratio revealed that it can be expressed as [51]

$$\Delta B(M1)/\langle B(M1)\rangle = \frac{4\cdot \Delta e' \cdot \hbar\omega}{(\Delta e')^2 + (\hbar\omega)^2}. \tag{8}$$

This equation should be valid for axially symmetric shapes in both the cranked shell model and the particle-rotor model, for the deformation-aligned bands, where K is a good quantum number. It has been shown [51] that for the high-Ω $\pi h_{11/2}$ bands in Ho, Tm, and Lu isotopes the left-hand side of the equation has a lower value than the right-hand side for negative γ deformations, and a higher value for positive γ deformations. On the basis of such a comparison, it has been suggested that the ^{157}Ho, ^{159}Tm, and ^{161,163,165}Lu deviate appreciably ($-15° \geqslant \gamma \geqslant -25°$) from an axially symmetric shape [51]. This is also observed for the $[514]9/2^-$ bands in the light Ta isotopes. In the case of ^{167}Ta, for example, the left- and right-hand sides of Eq. (8) have values of 0.28 and 0.79, respectively (calculated from the experimental data at $\hbar\omega \sim 0.27$). However, for the lighter ^{165}Ta, where the respective values are 0.32 and 1.17 (calculated from the experimental data at $\hbar\omega \sim 0.25$), this discrepancy is more pronounced. Such a trend is consistent with the assumption of increased γ instability of the nuclear shape with decreasing N and indicates a considerable negative γ deformation for ^{165}Ta.

It is therefore very likely that sizable deviations from axial symmetry cause the observed discrepancies between the experimental data, and theoretical calculations which assume an axially symmetric nuclear shape. Since CSM cannot properly treat nuclear γ softness, we performed such calculations with a fixed value of γ, representing the ''mean'' deviations from axial symmetry. A negative deformation with $\gamma = -18°$ not only raised the calculated crossing frequency to $\hbar\omega \sim 0.26$ with $\Delta i = 10.2\hbar$, (see the inset of upper part of Fig. 9), but also gave a very good agreement between the experimental signature splitting (69 keV at $\hbar\omega = 0.225$ MeV) and the theoretical value (67.1 keV, see the inset of the lower part of Fig. 9). Although according to Ref.

[51] the CSM is not quantitatively reliable when describing the low frequencies in triaxially deformed nuclei, the above results indicate that it is quite likely that a considerable triaxial nuclear deformation and/or increased γ softness plays a crucial role in the $\pi[514]9/2^-$ yrast band of ^{165}Ta.

V. SUMMARY AND CONCLUSIONS

The study of the nuclei in the rare-earth region has been extended with the spectroscopy of the most neutron-deficient tantalum nucleus investigated to date, ^{165}Ta, using the AFRODITE array. The yrast band of ^{165}Ta was established up to a spin of $\frac{53}{2}^-$. The band head was assigned $I^\pi = 9/2^-$ and the configuration $\pi[514]9/2^-$ was associated with the yrast band on the basis of systematics and cranked shell model calculations. According to total Routhian surface calculations the nuclear shape is expected to be γ soft. The alignment of the first $i_{13/2}$ pair of neutrons was found to occur at $\hbar\omega = 0.25$ MeV, below which a large signature splitting of the Routhians was observed for the $\Omega = 9/2$ yrast band. The splitting was found to almost disappear and become inverted above the backbend. CSM was unable to satisfactorily reproduce the experimentally observed band crossing frequency, nor the observed splitting in the Routhians or the $B(M1)/B(E2)$ ratios, if an axially symmetric nuclear shape was assumed. It is most likely that a substantial deviation from axial symmetry is the cause of these discrepancies.

ACKNOWLEDGMENTS

We would like to express our thanks to Ramon Wyss for providing us with the TRS code and for the stimulating discussions. The authors are also grateful to Rashid Nazmitdinov for helpful discussions. D.G.R. and G.K.M. acknowledge financial grants from both NAC and the University of Cape Town and NAC and National Research Foundation, respectively.

[1] W. Nazarewicz, M.A. Riley, and J.D. Garrett, Nucl. Phys. **A512**, 61 (1990).
[2] K. Theine, C.-X. Yang, A.P. Byrne, H. Hübel, R. Chapman, D. Clarke, F. Khazaie, J.C. Lisle, J.N. Mo, J.D. Garrett, and H. Ryde, Nucl. Phys. **A536**, 418 (1992).
[3] S.G. Li *et al.*, Nucl. Phys. **A555**, 435 (1993).
[4] J.C. Bacelar *et al.*, Nucl. Phys. **A442**, 547 (1985).
[5] C.-H. Yu, M.A. Riley, J.D. Garrett, G.B. Hagemann, J. Simpson, P.D. Forsyth, A.R. Mokhtar, J.D. Morrison, B.M. Nyakó, and J.F. Sharpey-Schafer, Nucl. Phys. **A489**, 477 (1988).
[6] Y. Ma, H. Sun, Y. Liu, S. Wen, H. Zheng, S. Li, G. Li, G. Yuan, P. Weng, and C. Yang, J. Phys. G **21**, 937 (1995).
[7] C.-H. Yu *et al.*, Nucl. Phys. **A511**, 157 (1990).
[8] P. Frandsen, R. Chapman, J.D. Garrett, G.B. Hagemann, B. Herskind, C.-H. Yu, K. Schiffer, D. Clarke, F. Khazaie, J.C. Lisle, J.N. Mo, L. Carlén, P. Ekström, and H. Ryde, Nucl. Phys. **A489**, 508 (1988).
[9] W. Schmitz, C.X. Yang, H. Hübel, A.P. Byrne, R. Müsseler, N. Singh, K.H. Maier, A. Kuhnert, and R. Wyss, Nucl. Phys. **A539**, 112 (1992).
[10] P. Frandsen *et al.*, Phys. Lett. B **177**, 287 (1986).
[11] S. Jónsson, J. Lyttkens, L. Carlén, N. Roy, H. Ryde, W. Waluś, J. Kownacki, G.B. Hagemann, B. Herskind, and J.D. Garrett, Nucl. Phys. **A422**, 397 (1984).
[12] C. Foin, D. Barnéoud, S.A. Hjorth, and R. Bethoux, Nucl. Phys. **A199**, 129 (1973).
[13] Y. Liu, Y. Ma, H. Yang, and S. Zhou, Phys. Rev. C **52**, 2514 (1995).
[14] S. Frauendorf and F.R. May, Phys. Lett. **125B**, 245 (1983).
[15] R. Bengtsson, H. Frisk, F.R. May, and J.A. Pinston, Nucl. Phys. **A415**, 189 (1984).
[16] R.M. Clark *et al.*, Appendix to Daresbury Annual Report, 37, 01990/91.
[17] J. Simpson, F. Hanna, M.A. Riley, A. Alderson, M.A. Bentley, A.M. Bruce, D.M. Cullen, P. Fallon, and L. Walker, J. Phys. G **18**, 1207 (1992).
[18] J. Simpson (private communication).
[19] R.T. Newman *et al.*, Balkan Phys. Lett. Special Issue, 182 (1998).
[20] K.S. Krane, R.M. Steffen, and R.M. Wheeler, Nucl. Data Tables **11**, 351 (1973).
[21] D.C. Radford, Nucl. Instrum. Methods Phys. Res. A **361**, 297 (1995).
[22] H. Zheng *et al.*, J. Phys. G **23**, 723 (1997).
[23] K.P. Blume *et al.*, Nucl. Phys. **A464**, 445 (1987).
[24] N.G. Nicolis, D.G. Sarantites, and J.R. Beene, computer code EVAP (unpublished).
[25] P.M. Jones, L. Wei, F.A. Beck, P.A. Butler, T. Byrski, G. Duchêne, G. de France, F. Hannachi, G.D. Jones, and B. Kharraja, Nucl. Instrum. Methods Phys. Res. A **362**, 556 (1995).
[26] E. Gueorguieva, C. Schück, Ch. Vieu, J.J. Correia, J.S. Dionisio, A. Minkova, M. Kaci, and B. Kharraja, Balkan Phys. Lett. Special Issue, 267 (1998).
[27] F.G. Kondev, G.D. Dracoulis, A.P. Byrne, M. Dasgupta, T. Kibédi, and G.J. Lane, Nucl. Phys. **A601**, 195 (1996).
[28] D.E. Archer *et al.*, Phys. Rev. C **52**, 1326 (1995).
[29] F.G. Kondev, G.D. Dracoulis, A.P. Byrne, T. Kibédi, and S. Bayer, Nucl. Phys. **A617**, 91 (1997).
[30] R.B. Firestone, *Table of Isotopes*, 8th ed. (Wiley, New York, 1996) (^{167}Ta and ^{169}Ta); Evaluated Nuclear Structure Data Files, National Nuclear Data Center, Brookhaven National Laboratory:
www.nndc.bnl.gov (^{171}Ta and ^{179}Ta).
[31] R. Bengtsson and S. Frauendorf, Nucl. Phys. **A327**, 139 (1979).
[32] I. Hamamoto, Nucl. Phys. **A520**, 297c (1990).
[33] R.A. Bark, G.D. Dracoulis, A.E. Stuchbery, A.P. Byrne, A.M. Baxter, F. Riess, and P.K. Weng, Nucl. Phys. **A501**, 157 (1989).
[34] W. Nazarewicz, G.A. Leander, and J. Dudek, Nucl. Phys. **A467**, 437 (1987).
[35] W. Nazarewicz, J. Dudek, R. Bengtsson, T. Bengtsson, and I.

Ragnarsson, Nucl. Phys. **A435**, 397 (1985).
[36] G. Andersson *et al.*, Nucl. Phys. **A268**, 205 (1976).
[37] R. Wyss, F. Lidén, J. Nyberg, A. Johnson, D.J.G. Love, A.H. Nelson, D.W. Banes, J. Simpson, A. Kirwan, and R. Bengtsson, Nucl. Phys. **A503**, 244 (1989).
[38] R. Wyss, J. Nyberg, A. Johnson, R. Bengtsson, and W. Nazarewicz, Phys. Lett. B **215**, 211 (1988).
[39] H. Schnack-Petersen *et al.*, Nucl. Phys. **A594**, 175 (1995).
[40] J. Dudek, Z. Szymański, and T. Werner, Phys. Rev. C **23**, 920 (1981).
[41] R. Bengtsson, J. Dudek, W. Nazarewicz, and P. Olanders, Phys. Scr. **39**, 1996 (1989).
[42] T. Bengtsson and I. Ragnarsson, Nucl. Phys. **A436**, 14 (1985).
[43] F. Dönau, Nucl. Phys. **A471**, 469 (1987).
[44] K. Alder, A. Bohr, T. Huus, B. Mottleson, and A. Winther, Rev. Mod. Phys. **28**, 432 (1956).
[45] O. Prior, F. Boehm, and S.G. Nilsson, Nucl. Phys. **A110**, 257 (1968).
[46] S. Frauendorf, Phys. Lett. **100B**, 219 (1981).
[47] H. Emling, E. Grosse, R. Kulessa, D. Schwalm, and H.J. Wollersheim, Nucl. Phys. **A419**, 187 (1984).
[48] M. Fewell *et al.*, Phys. Rev. C **31**, 1057 (1985).
[49] M. Fewell *et al.*, Phys. Rev. C **37**, 101 (1988).
[50] J.C. Bacelar, A. Holm, R.M. Diamond, E.M. Beck, M.A. Deleplanque, J. Draper, B. Herskind, and F.S. Stephens, Phys. Rev. Lett. **57**, 3019 (1986).
[51] G.B. Hagemann and I. Hamamoto, Phys. Rev. C **40**, 2862 (1989).
[52] I. Hamamoto, *Proceedings of the Workshop on Microscopic Models in Nuclear Structure Physics*, Oak Ridge (World Scientific, Singapore, 1988), p. 173.
[53] S. Jónsson, N. Roy, H. Ryde, W. Walus, J. Kownacki, J.D. Garrett, G.B. Hagemann, B. Herskind, R. Bengtsson, and S. Åberg, Nucl. Phys. **A449**, 537 (1986).
[54] Y-J. Ma *et al.*, J. Phys. G **26**, 43 (2000).
[55] R.A. Bark *et al.*, Nucl. Phys. **A644**, 29 (1998).
[56] L. Funke, K-H. Kaun, P. Kemnitz, H. Sodan, and G. Winter, Nucl. Phys. **A170**, 593 (1971).
[57] D.C. Radford, A. Galindo-Uribarri, V.P. Janzen, D. Ward, S. Flibotte, S.M. Mullins, J.C. Waddington, M. Cromaz, J. de Graaf, and T.E. Drake, Proceedings of the Conference on Nuclear Structure at the Limits, Argonne, Illinois, 1996.
[58] A.G. Smith *et al.*, Nucl. Phys. **A587**, 150 (1995).
[59] H.J. Jensen *et al.*, Z. Phys. A **340**, 351 (1991).
[60] J. Simpson, M.A. Riley, A. Alderson, M.A. Bentley, A.M. Bruce, D.M. Cullen, P. Fallon, F. Hanna, and L. Walker, J. Phys. G **17**, 511 (1991).
[61] J.D. Garrett *et al.*, Phys. Rev. Lett. **47**, 75 (1981).
[62] W.F. Mueller, H.J. Jensen, W. Reviol, L.L. Riedinger, C.-H. Yu, J.-Y. Zhang, W. Nazarewicz, and R. Wyss, Phys. Rev. C **50**, 1901 (1994).
[63] G.B. Hagemann, J.D. Garrett, B. Herskind, G. Sletten, P.O. Tjøm, A. Henriquez, F. Ingebretsen, J. Rekstad, G. Løvhøiden, and T.F. Thorsteinsen, Phys. Rev. C **25**, 3224 (1982).
[64] G.B. Hagemann, J.D. Garrett, B. Herskind, J. Kownacki, B.M. Nyakó, P.L. Nolan, J.F. Sharpey-Schafer, and P.J. Tjøm, Nucl. Phys. **A424**, 365 (1984).
[65] A.J. Larabee and J.C. Waddington, Phys. Rev. C **24**, 2367 (1981).
[66] I. Hamamoto and B.R. Mottelson, Phys. Lett. **132B**, 7 (1983).
[67] J. Gascon, P. Taras, D.C. Radford, D. Ward, H.R. Andrews, and F. Banville, Nucl. Phys. **A467**, 539 (1987).